applied optics

Wavelength stabilization and spectra narrowing of a 405 nm external-cavity semiconductor laser based on a volume Bragg grating

Ye Liu,[1] Yu Liu,[1] Hongling Li,[1] Huidong Xiao,[1,*] Yingkai Xia,[1] Ruihong Gao,[1] Xiang Li,[1] and Quan Zheng[1,2]

[1]Changchun New Industries Optoelectronics Technology Co., Ltd, Changchun, Jilin 130012, China
[2]Changchun Institute of Optics, Fine Mechanics and Physics, Chinese Academy of Science, Changchun, Jilin 130033, China
*Corresponding author: xiaohd@cnilaser.com

Received 11 February 2022; revised 22 April 2022; accepted 23 April 2022; posted 25 April 2022; published 9 May 2022

We introduce a 405 nm external-cavity semiconductor laser using a volume Bragg grating (VBG) as the feedback element. By decreasing the length of the external cavity and reducing the wavelength difference between the output wavelength of the laser diode during free running and Bragg wavelength of the VBG, the emission wavelength of the semiconductor laser is stably locked at 405.1 nm with a spectral linewidth of 0.08 nm. The output power reaches 292 mW, and the wavelength drift with temperature reduces to 0.0006 nm/°C. These results are helping for the spectroscopy applications of a blue-violet laser diode. In contrast to traditional external-cavity semiconductor lasers, this laser is less expensive and more compact, in addition to having a narrow linewidth and good wavelength stability. These advantages would facilitate the development of associated areas of research, including optical data storage, laser display, and laser medicine.

https://doi.org/10.1364/AO.456078

1. INTRODUCTION

Semiconductor lasers have the advantages of small size, high efficiency, and low cost, and they are widely used in various applications, such as infrared scientific research, remote sensing, Raman spectroscopy, and medical fields [1,2]. However, certain deficiencies in their performance have become critical for several demanding applications [3,4]. The wavelength drifts of semiconductor lasers vary remarkably with temperature (by approximately 0.1 nm/°C) and current, and their spectral linewidth [full width at half-maximum (FWHM)] is excessively broad (1–4 nm). Therefore, several attempts have been made to develop semiconductor lasers with narrow spectral linewidths and stable central wavelengths. Optical feedback techniques have generally been employed to improve the optical properties of semiconductor lasers [5–7]. Typical lasers with optical feedback techniques include distributed feedback (DFB) and distributed Bragg reflector (DBR) semiconductor lasers [8,9], which can achieve a stabilized central wavelength and narrow spectral linewidth. Nevertheless, DFB and DBR lasers have the disadvantages of complicated fabrication processes, high cost, and low power. In addition, conventional external cavity diode laser (ECDL) designs such as the Littrow and Littman–Metcalf configurations use surface gratings for wavelength selection [10–15]. In 2014, Ruhnke *et al*. reported a 445 nm ECDL with an output power of up to 400 mW and a linewidth of approximately 20 pm [14]. A tunable 410 nm ECDL was demonstrated by Li *et al*. in 2017, with an output power of 500 mW and a linewidth of approximately 50 pm [15]. In 2021, Nyaupane *et al*. proposed two broad-area laser diodes (445 nm) employing a common external cavity consisting of the surface grating in a Littrow configuration [13]. The spectral linewidth of the combined laser beam was reduced to 10–15 pm, and the total combined power was more than 1 W. However, these lasers are structurally unstable owing to their extreme sensitivity to temperature and mechanical vibrations [16–18].

In recent years, volume Bragg gratings (VBGs) have been utilized as feedback elements to achieve wavelength-locked semiconductor lasers to compensate for the shortcomings of free-running semiconductor lasers. VBGs recorded in photothermal refractive (PTR) glass can be tailored to supply reflection coefficients of up to ∼99% with relatively narrow linewidths (<0.2 nm), shallow residual loss owing to scattering and absorption, and high damage thresholds [19–21]. Owing to these properties, VBGs are commonly utilized for optimizing semiconductor lasers [22–25]. In 2004, Volodin *et al*. reported narrow-linewidth laser output from multimode laser diodes (LDs) and arrays at 785 nm using a VBG and improved the wavelength stability of the semiconductor lasers by a factor of approximately 30 [26]. Paboeuf *et al*. (2008) studied VBG-locked conical semiconductor laser arrays at 976 nm with a narrow spectral linewidth (100 pm) and an output power of 1.7 W [7]. Additionally, Liu *et al*. (2019) studied red-light

external-cavity semiconductor lasers using a reflecting VBG [27]. The linewidth of the output spectrum was compressed to approximately 0.7 nm, and the output power was 1.06 W. Most previous applications of VBGs focused on multimode LDs with an emitting aperture in the 100–200 μm range and near-infrared wavelengths [7,26–29]. Blue-violet semiconductor lasers based on VBGs are rarely mentioned. Ruhnke *et al*. (2016) reported a micro-integrated ECDL module with a holographic VBG at 445 nm, with an output power of up to 1.4 W and a linewidth of approximately 50 pm [30]. Moser *et al*. proposed a novel self-aligned non-dispersive external cavity laser of 405 nm based on the volume holographic gratings [31,32]. The findings demonstrated that the output power was less than 10 mW. Although 405 nm ECDLs with volume holographic gratings have been reported in some studies, the research has primarily focused on one aspect of spectral properties. Thus, more studies are required for the analysis of comprehensive spectral properties of lasers with grating feedback.

In this study, we demonstrate a 405 nm external-cavity semiconductor laser with an emitting aperture of 30 μm, which adopts a VBG to achieve a stabilized wavelength and narrow spectral linewidth. This study thoroughly analyzes the improvement of the spectral characteristics of a 405 nm semiconductor laser based on the VBG. Here an optical power of 292 mW with a narrowband emission of 0.08 nm and a wavelength drift of 0.0006 nm/°C is achieved. With the advantages of a stabilized central wavelength, narrow spectral linewidth, compactness, and robustness, the laser demonstrated in this study is valuable and significant for applications in several fields, such as high-capacity optical data storage [33], laser display [34], laser medicine [35], and advanced manufacturing [36,37], and so on.

2. EXPERIMENTAL SETUP

A linear external-cavity semiconductor laser was constructed using a reflecting VBG as shown in Fig. 1. A transistor outline (TO)-package LD (NDV4B16, NICHIA) with a light-emitting area of only 30 μm was adopted, with a wavelength centered at ~405 nm, with no further AR coating on its output facet. The spectral emission width was approximately 1 nm (FWHM). An aspherical lens was used to collimate the divergent beam output from the LD to achieve optimal coupling. The selected aspherical lens was made by Lightpath, Inc. (with focal length $f = 4.02$ mm and numerical aperture NA = 0.6) with an AR coating from 400 to 700 nm. Owing to the different far-field angles in the lateral and vertical directions, the collimated beam had an elliptic shape of 2.6 mm × 1.2 mm. The reflecting VBG was fabricated by Optigrate with a diffraction efficiency of 35% (η_0) and spectral bandwidth of 0.1 nm (λ_{FWHM}). The VBG has an aperture of 3.5 mm × 3 mm and a thickness of 1.2 mm (t). The Bragg wavelength (λ_0) of the VBG is 405.1 nm at 25°C. A high-precision six-axis rotation platform was used to precisely adjust the spatial position of the VBG. The entire setup was mounted on a thermoelectrically cooled copper heat sink with a temperature accuracy of 0.1°C. The resolution of the fiber-coupled spectrum analyzer (Changchun New Industry Optoelectronics Technology Co., Aurora 4000) was 0.1 nm (FWHM).

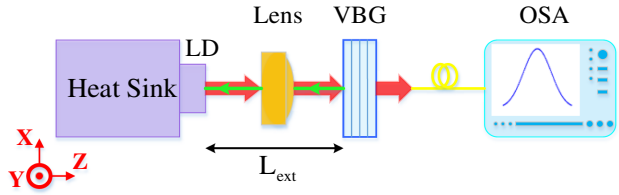

Fig. 1. Experimental setup of the external-cavity semiconductor laser based on a VBG.

3. THEORETICAL ANALYSIS AND SIMULATION

A reflecting VBG was used for wavelength stabilization. Figure 2 shows the principle of VBG.

Selective diffraction occurs only at a specific incident angle and wavelength when a VBG is inserted into the laser beam path. Because of the intrinsic wavelength and angular selectivity, the use of a VBG inside an external cavity may modify the propagation of the laser beam and reduce the effective coupling coefficient. To model their effects on the mode selectivity of the external cavity, the reflectivity and transmission of the Bragg grating must be considered. The spectral selectivity of a reflecting VBG is determined by the number of Bragg planes that the light traverses inside the glass [26]:

$$\frac{\lambda_{\mathrm{FWHM}}}{\lambda_0} = \frac{\lambda_0}{2n_{av}t} = \frac{\Lambda}{t} = \frac{1}{N}, \tag{1}$$

where $\Lambda = 1/f$ denotes the period of the grating (Fig. 2), f is the grating spatial frequency of the grating, n_{av} is the bulk refractive index, and N is the number of grating planes that fit the thickness of the material. For VBGs, the diffraction of a beam with a particular wavelength occurs at only a specific angle, which depends on the grating spatial frequency of the grating according to Bragg's condition [38]

$$|\cos\theta_B| = \frac{\lambda_0 f}{2n_{av}}, \tag{2}$$

where θ_B denotes the conventional Bragg angle in media. According to Kogelink's theory [39], the diffraction efficiency of an unslanted Bragg grating is described by the following formula:

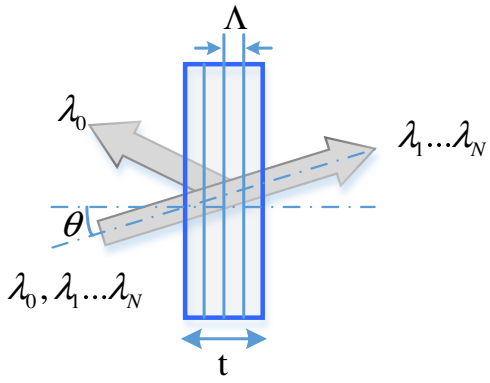

Fig. 2. Schematic of a reflecting VBG.

$$\eta(\Delta\lambda)=\left\{1+\frac{1-\left(\frac{\lambda_0 f^2\Delta\lambda}{2n_{av}\delta n}\right)^2}{\sinh^2\left[\left(\frac{2\pi n_{av}t\delta n}{\lambda_0{}^2 f}\right)^2-\left(\frac{\pi f t\Delta\lambda}{\lambda_0}\right)\right]^{1/2}}\right\}^{-1}, \tag{3}$$

where $\Delta\lambda=\lambda-\lambda_0$ denotes the wavelength difference of the incident laser wavelength (λ) and the Bragg wavelength (λ_0). δn denotes the amplitude of refractive index modulation. When the incident light enters the VBG at an angle θ (Fig. 1), $\Delta\theta=\theta-\theta_B$ denotes the angular difference of the incident and Bragg angles. According to Eq. (2), the interrelation between wavelength and angular parameters can be obtained as follows:

$$\frac{\Delta\theta}{\Delta\lambda}=\frac{f}{2n_{av}\cos\theta_B}. \tag{4}$$

When the exact Bragg condition ($\Delta\theta=\Delta\lambda=0$) is satisfied, the maximum diffraction efficiency of VBG can be simplified from Eq. (3) as follows:

$$\eta_0=\tanh^2\frac{2\pi n_{av}t\delta n}{\lambda_0{}^2 f}, \tag{5}$$

where η_0, t, λ_0, and λ_{FWHM} are provided, and n_{av}, f, and δn can be calculated from Eq. (1) and (5), respectively. Using theoretical simulations, the wavelength and angle selectivities are shown simultaneously in Fig. 3. The experimental LD and aspherical lens were introduced in Section 2. The spectral emission width was approximately 1 nm (FWHM). The far-field divergence angles (FWHM) of laser diode emission were <0.5 mrad in horizontal and vertical directions. The peak diffraction efficiency of the VBG was up to 35%, which was achieved when the Bragg condition was satisfied. The excellent wavelength (FWHM = 0.1 nm) and sensitive angular (FWHM = 0.24°) selectivities of the VBG are the foundations of the wavelength-locking experiment.

Figure 4 shows the spectral selectivity of a reflecting VBG for the theoretical simulation and experimental measurements. The actual spectral width and diffraction efficiency of this external-cavity mirror is 0.1 nm and 35%, respectively. The spectral width (FWHM) of the filter coincided with the theoretical value with an accuracy of a few percent. However, the sidelobes of the

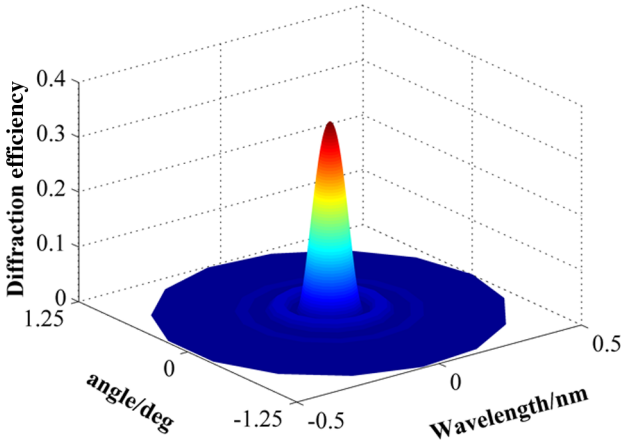

Fig. 3. Dependence of diffraction efficiency on wavelength and angle selectivity.

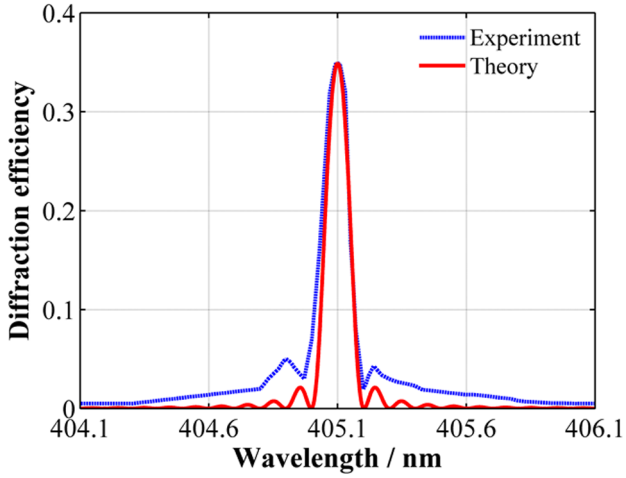

Fig. 4. Spectral selectivity of a reflecting VBG at 405.1 nm.

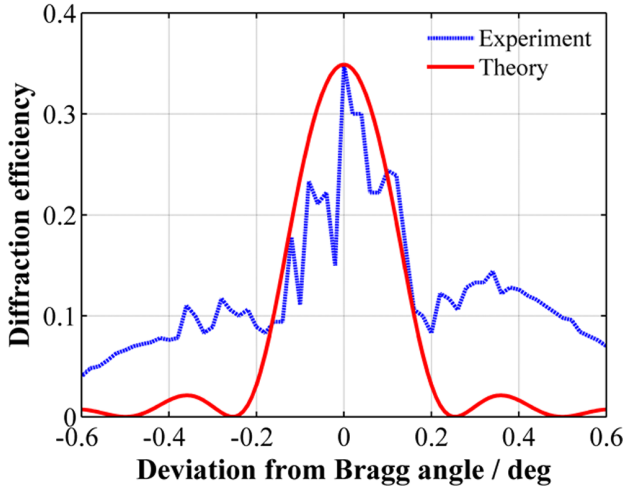

Fig. 5. Angle selectivity of a reflecting VBG at 405.1 nm.

reflectivity curve were smeared because of the wide emission spectrum of the experimental LD [38].

Figure 5 shows the angular selectivity of the reflecting VBG for the theoretical simulation and experimental measurements. The envelope of the experimental profiles of the diffraction efficiency approximately coincided with the theoretical value for VBG. The angular selectivity was approximately 4.19 mrad (FWHM = 0.24°) for the PTR Bragg grating with a thickness of 1.2 mm. Notably, the experimental data and theoretical simulation do not match well. This is probably due to the uneven value of the refractive index modulation across the aperture of the hologram [40] and the mismatch between the aperture of VBG and the beam aperture [38]. Overall, the experimental peak diffraction efficiencies of the tested data matched well with the theoretical values.

4. RESULTS AND DISCUSSION

A. Output Properties of VBG-Locked Laser

Figure 6 shows the emission spectra of the 405 nm LD measured at 300 mA driving current; the blue line represents the

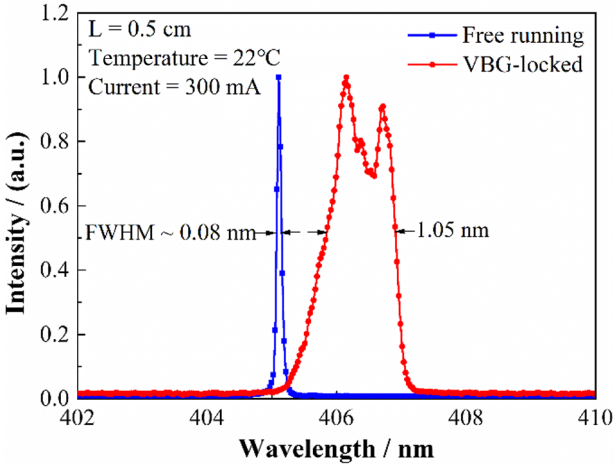

Fig. 6. Comparison of the output spectra of a free-running and VBG-locked laser.

free-running status, whereas the red line represents the VBG-locked status. Each spectrum was normalized in intensity to 1, and all the spectra were presented in a contour diagram. The cavity length (L_{ext}) was 0.5 cm, and the heat-sink temperature was set as 22°C. The maximum wavelength of the free-running LD was ~406.8 nm with a spectral width of 1.05 nm (FWHM). By contrast, the VBG-locked laser had a much narrower lasing spectrum of 0.08 nm centered at 405.1 nm. To narrow the spectral bandwidth, only the spectral components selected by the VBG are fed back to the active area of the LD. In this external-cavity configuration, the rear facet of the emitting element acts as an end mirror, and the VBG serves as an output mirror. We achieved wavelength stabilization and spectrum narrowing of a semiconductor laser with a single external cavity by simply using a VBG. Figure 7 shows the output power of the free-running (blue line) and VBG-locked (red line) lasers versus the driving current. At this time, the cavity length and heat-sink temperature were fixed. When aligned, the slope efficiency for the VBG-locked laser was 85% that of the LD when free-running. Notably, these two main factors cause a decrease in the slope efficiency. On the one hand, the feedback light from the VBG was not all incident into the LD active region, resulting

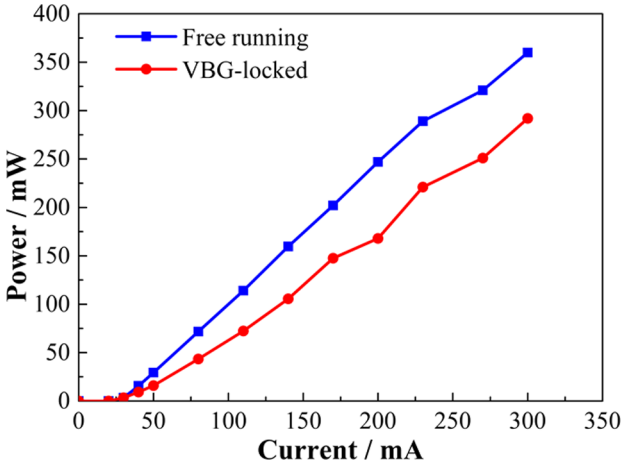

Fig. 7. Comparison of the output power versus driving current of free-running and VBG-locked lasers.

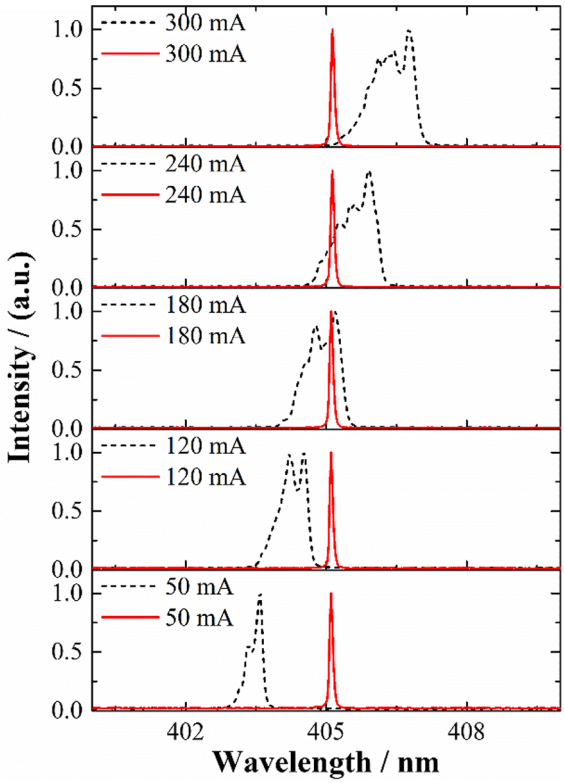

Fig. 8. Emission spectra versus currents of free-running and VBG-locked lasers.

in scattering losses. On the other hand, waveguide losses in the LD cavity led to optical losses.

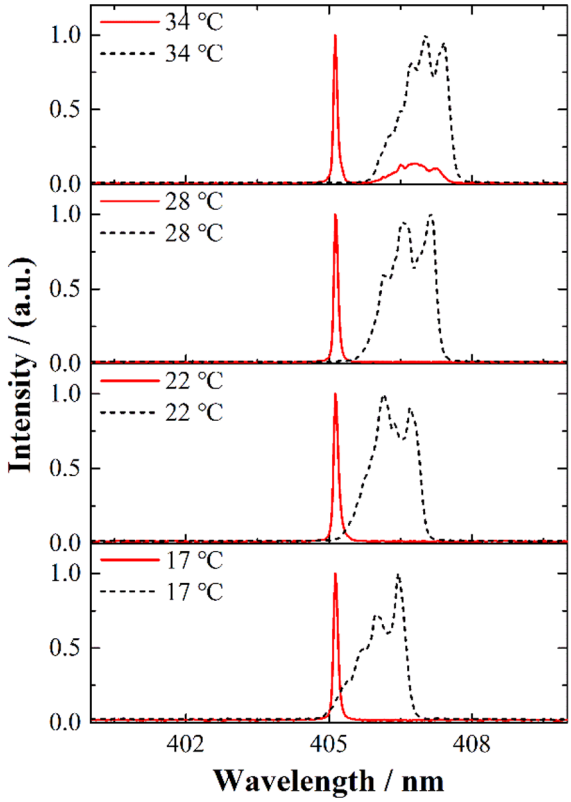

Fig. 9. Emission spectra versus temperatures of free-running and VBG-locked lasers.

In order to make a clear comparison, the emission spectra of a free-running (dashed line) and the VBG-locked laser (solid line) at different driving currents are presented in Fig. 8. At this time, the cavity length and heat-sink temperature were fixed. With the increasing current, the spectra of the free-running LD showed remarkable broadening and redshift. This was caused by the temperature change in gain medium with increasing driving current, which led to the change of effective refractive index and resonator length. Owing to the stable feedback from the VBG, the laser achieved stable and narrow linewidth emission compared to the free-running LD. A bare LD had a broad emission spectrum of several nanometers. The VBG laser can have a wavelength outside of the extensive luminescence bands. Furthermore, we materialized the same remarkable wavelength-locked effect with the heat-sink temperatures of 28°C and 31°C. Figure 9 shows the emission spectra of a free-running (dashed line) and the VBG-locked laser (solid line) at different heat-sink temperatures. At this time, the cavity length and driving current were fixed. Likewise, the free-running wavelength also exhibited a prominent redshift with increasing temperature. The peak wavelength of the VBG-locked laser was stably locked at the Bragg wavelength (405.1 nm). The edge modes of the spectra appeared in the longwave direction (407.5 nm) of the Bragg wavelength at a temperature of 34°C.

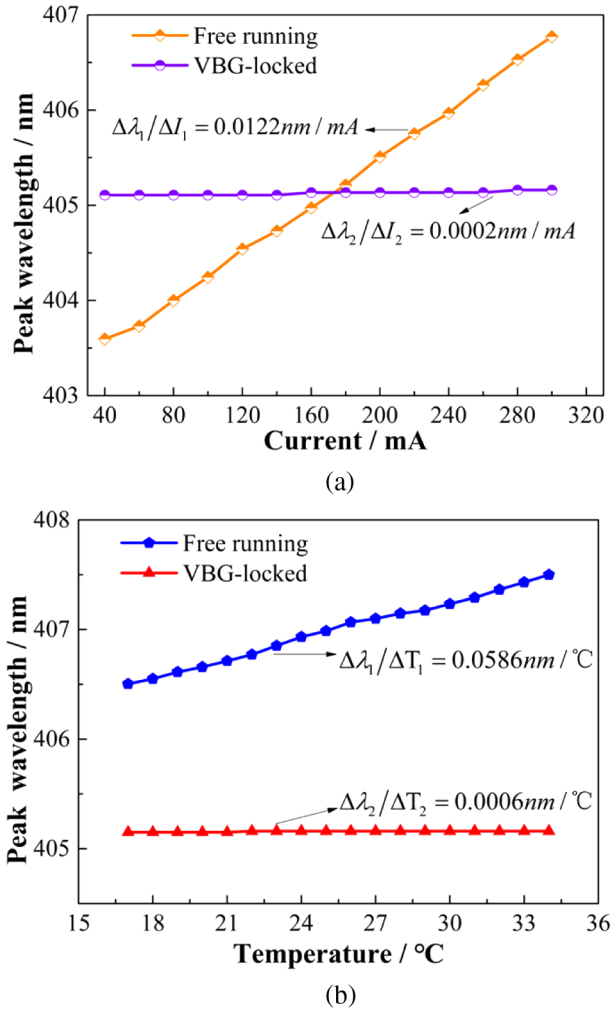

Fig. 10. Comparison of stabilization of peak wavelength when free-running and VBG-locked versus (a) driving current and (b) heat-sink temperature.

The heat-sink temperature was set as 22°C. The peak wavelength shift decreased from 0.0122 to 0.0002 nm/mA owing to the locking of the wavelength by a VBG [see Fig. 10(a)]. Figure 10(b) illustrates the peak wavelength versus temperature in different cases. When the driving current was 300 mA, the wavelength drift gradually reduced from 0.0586 to 0.0006 nm/°C. The wavelength drift was degraded by a factor of approximately 97 by a VBG.

B. Wavelength Locking and Spectra Narrowing of the 405 nm LD

Wavelength stabilization and spectrum narrowing can be achieved under specific conditions, such as by matching the cavity length, driving current, and heat-sink temperature. According to the theoretical analysis of the wavelength selection characteristics of the VBG discussed in Section 3, the most critical factor is the match between the reflection spectrum of the VBG and the gain spectrum of the LD. In essence, wavelength locking depends on the competition between the frequency selection function of the surface feedback of the cavity and the LD gain spectrum itself. However, the gain spectrum of the LD depends on the driving current and heat-sink temperature.

The spectra at a cavity length from 0.5 to 2 cm were measured at a temperature of 22°C and a current of 300 mA as shown in Fig. 11. As the cavity length increased, the spectral linewidth became progressively wider. When the cavity length reached 2 cm, a significant edge mode appeared near the peak wavelength. This phenomenon was due to the specific angular selectivity of the VBG, and the beam divergence angles were

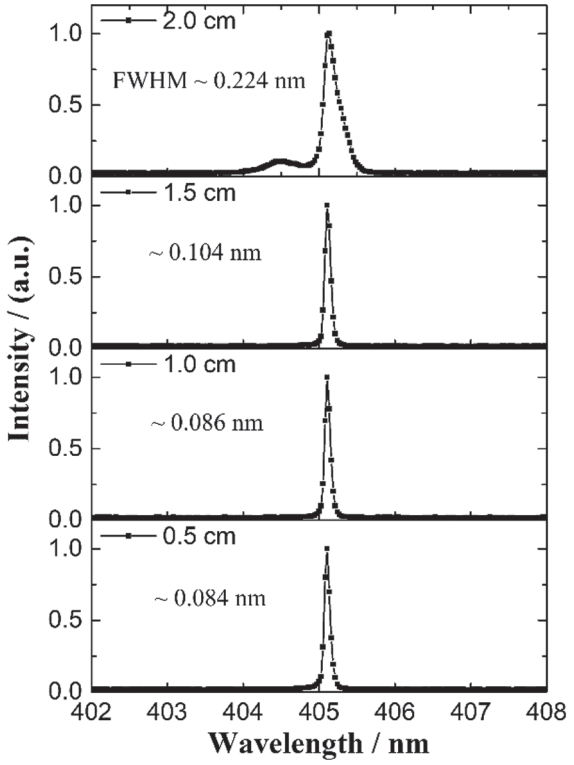

Fig. 11. Emission spectra of VBG-locked laser under different cavity lengths.

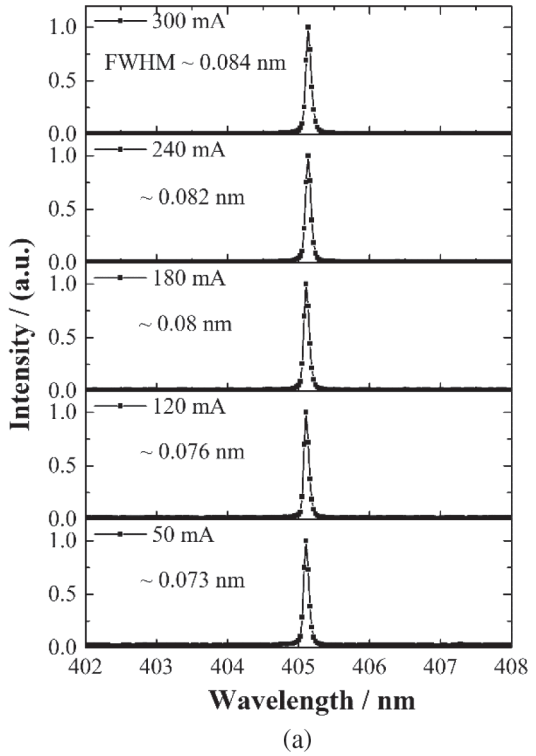

Fig. 12. Emission spectra versus current of VBG-locked laser at temperatures of (a) 22°C and (b) 34°C.

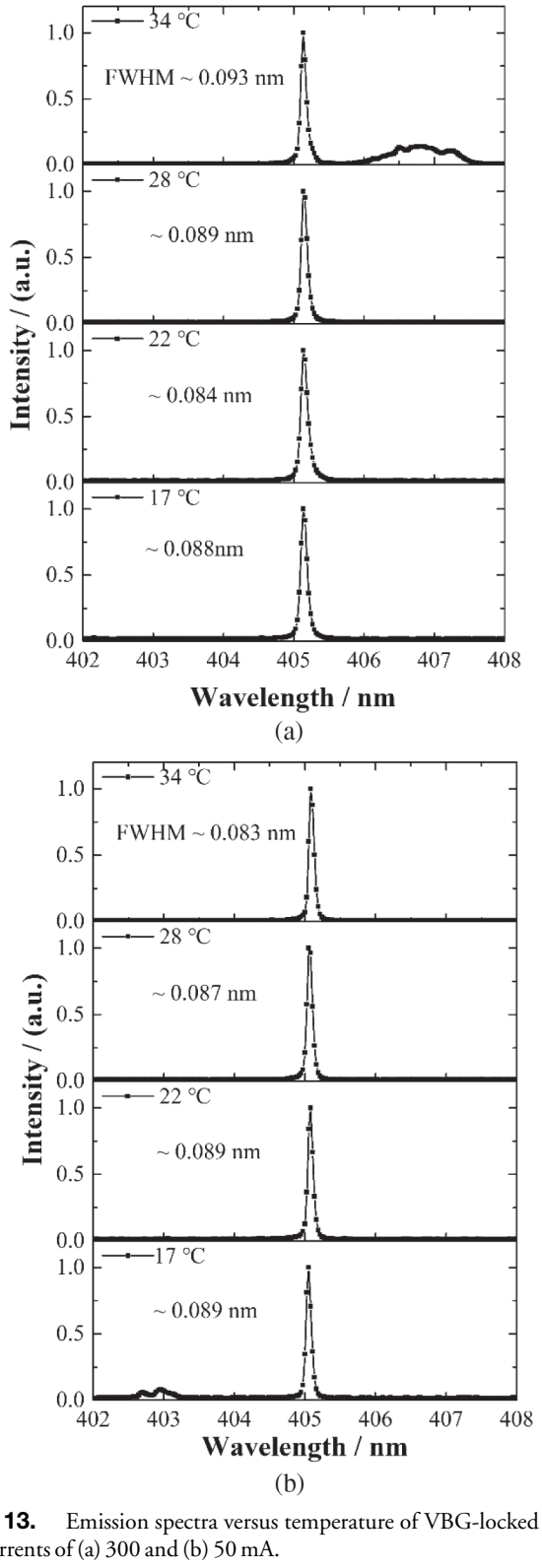

Fig. 13. Emission spectra versus temperature of VBG-locked laser at currents of (a) 300 and (b) 50 mA.

different for far-field transverse modes of different orders. The collimated beam contained the fundamental transverse mode beam and the other order transverse mode beams. The beam divergence angle was the smallest for the fundamental transverse mode, and the divergence angles increased as the order increased in the transverse modes. When different transverse modes are incident at different angles, a higher-order transverse mode beam cannot be effectively fed back into the active area of the chip because of the finite acceptance angle of the VBG, resulting in an optical loss. In subsequent research, the cavity length was

adjusted to be as short as that of the collimating lens, and the VBG distance was allowed (0.5 cm).

Figures 12(a) and 12(b) show a comparison of the emission spectra and current at the heat-sink temperatures of 22°C and 34°C. The laser remained locked at all current values and 22°C [see Fig. 12(a)]. However, when the heat-sink temperature was regulated to 34°C, the outcomes were not identical in Fig. 12(b). The mode of the LD internal cavity oscillations was magnified as soon as the current increased to 300 mA. As the driving current increased, the spectral showed remarkable broadening. The longer emission wavelength of the semiconductor laser was demonstrated with higher temperatures and driving currents.

Figures 13(a) and 13(b) show a comparison of the emission spectra and the heat-sink temperature at driving currents 50 and 300 mA. The edge modes of the spectra appeared in the longwave direction (407.5 nm) of the Bragg wavelength at a temperature of 34°C and a current of 300 mA as shown in Fig. 13(a). Nevertheless, the edge modes appeared in the shortwave direction (at 402.6 nm) of the Bragg wavelength at a temperature of 17°C and a current of 50 mA in Fig. 13(b). The narrowband feedback provided by the VBG cannot overwhelm the wavelength difference (2.5 nm) between the emission wavelength of the LD and Bragg wavelength. As the wavelength difference increased, the spectral linewidth became progressively broader. The shorter emission wavelength of the semiconductor laser was demonstrated with lower temperatures and driving currents.

The results demonstrated an excellent wavelength-locked effect for a shorter external cavity length in the practical application of semiconductor lasers. The wavelength-locked effect was also affected by the difference between the free-running wavelength of the LD and the Bragg wavelength of the VBG. It worsened when the difference was longer than 2.5 nm. The empirical analysis enabled us to understand the intimate relationship between the emission wavelength with the driving current and heat-sink temperature. To obtain a more stable wavelength and narrower linewidth, the wavelength of the semiconductor laser can only be brought closer to the Bragg wavelength simply by modulating the current and temperature to suitable parameters.

5. CONCLUSION

A reflection VBG was established as an optical feedback element for laser design to stabilize the wavelength significantly (by a factor of 97) and narrow the emission spectra (by a factor of 13) of semiconductor lasers in this study. This study comprehensively examined the improvement of the spectral characteristics of a 405 nm semiconductor laser based on the VBG. A detailed theoretical and experimental analysis based on the spectral and angular properties of VBGs was used to model their effects on the mode selectivity of an external cavity. Using the idea, we demonstrated that narrowband feedback from a VBG simultaneously achieved the wavelength locking, linewidth narrowing, and stabilization of the peak wavelength against the driving current (drift of ~0.0002 nm/mA) and heat-sink temperature (drift of ~0.0006 nm/°C). It was also observed that the spectra were perfectly optimized when we adjusted the current and temperature to decrease the difference in wavelength between the emission wavelength of the LD and Bragg wavelength. The wavelength-locked effect deteriorates when the difference is longer than 2.4 nm. The external-cavity semiconductor laser at the blue-violet wavelength designed in this study has the advantages of low cost, narrow linewidth, excellent wavelength stability, and compact structure, and it can be applied in fields such as optical data storage, laser displays, and laser medicine. This technique is suitable for application to other wavelength ranges. In our experiments, the spectra linewidth was narrowed to 0.08 nm. Therefore, we believe it will be possible to further decrease the spectral bandwidth with a properly designed VBG and laser chip.

Funding. Jilin Scientific and Technological Development Program (20200401072GX).

Disclosures. The authors declare no conflicts of interest.

Data availability. The data that supports the findings of this study are available within the article.

REFERENCES

1. A. M. Haughey, G. M. Connell, B. Guilhabert, G. A. Burley, M. D. Dawson, and N. Laurand, "Organic semiconductor laser biosensor: design and performance discussion," IEEE J. Sel. Top. Quantum **22**, 1300109 (2015).
2. P. J. Rodrigo and C. Pedersen, "Field performance of an all-semiconductor laser coherent Doppler lidar," Opt. Lett. **37**, 2277–2279 (2012).
3. M. J. Chi, O. B. Jensen, and P. M. Petersen, "Tuning range and output power optimization of an external-cavity GaN diode laser at 455 nm," Appl. Opt. **55**, 2263–2269 (2016).
4. S. R. Oh, J. H. Park, K. Kim, E. S. Lee, J. Y. Lee, and S. Kim, "Investigation of fiber Bragg grating as a spectral notch shaper for single-pulse coherent anti-Stokes Raman spectroscopy," Opt. Commun. **383**, 107–112 (2017).
5. B. Dahmani, L. Hollberg, and R. Drullinger, "Frequency stabilization of semiconductor lasers by resonant optical feedback," Opt. Lett. **12**, 876–878 (1987).
6. S. K. Turitsyn, S. A. Babin, A. E. El-Taher, P. Harper, D. V. Churkin, S. I. Kablukov, J. D. Ania-Castanon, V. Karalekas, and E. V. Podivilov, "Random distributed feedback fiber laser," Nat. Photonics **4**, 231–235 (2010).
7. D. Paboeuf, G. Lucas-Leclin, P. Georges, N. Michel, M. Krakowski, J. Lim, S. Sujecki, and E. Larkins, "Narrow-line coherently combined tapered laser diodes in a Talbot external-cavity with a volume Bragg grating," Appl. Phys. Lett. **93**, 211102 (2008).
8. Y. Sun, F. Wei, Z. Dong, D. Chen, H. Cai, and R. Qu, "All-optical frequency stabilization and linewidth reduction of distributed feedback diode lasers by polarization rotated optical feedback," Opt. Express **22**, 15757–15762 (2014).
9. K. D. Singer, T. Kazmierczak, J. Lott, H. Song, Y. Wu, J. Andrews, E. Baer, A. Hiltner, and C. Weder, "Melt-processed all-polymer distributed Bragg reflector laser," Opt. Express **16**, 10358–10363 (2008).
10. Q. Lv, Z. Liu, W. Wang, X. Li, S. Li, Y. Song, H. Yu, A. Bayanheshig, and W. Li, "Simple and compact grating-based heterodyne interferometer with the Littrow configuration for high-accuracy and long-range measurement of two-dimensional displacement," Appl. Opt. **57**, 9455–9463 (2018).
11. X. Q. Lv, S. W. Chen, J. Y. Zhang, L. Y. Ying, and B. P. Zhang, "Tuning properties of external cavity violet semiconductor laser," Chin. Phys. Lett. **30**, 074204 (2013).
12. D. Ding, X. Lv, X. Chen, F. Wang, J. Zhang, and K. Che, "Tunable high-power blue external cavity semiconductor laser," Opt. Laser Technol. **94**, 1–5 (2017).
13. P. R. Nyaupane, P. L. LikamWa, and Y. Braiman, "Spectral linewidth narrowing of two broad area blue laser diodes (445 nm) with a common external cavity," Opt. Lett. **46**, 2718–2721 (2021).

14. N. Ruhnke, A. Müller, B. Eppich, M. Maiwald, B. Sumpf, G. Erbert, and G. Tränkle, "400 mW external cavity diode laser with narrowband emission at 445 nm," Opt. Lett. **39**, 3794–3797 (2014).
15. B. Li, J. Gao, A. Yu, S. Luo, D. Xiong, X. Wang, and D. Zuo, "500 mW tunable external cavity diode laser with narrow line-width emission in blue-violet region," Opt. Laser Technol. **96**, 176–179 (2017).
16. X. Baillard, A. Gauguet, S. Bize, P. Lemonde, P. Laurent, A. Clairon, and P. Rosenbusch, "Interference-filter-stabilized external-cavity diode lasers," Opt. Commun. **266**, 609–613 (2006).
17. D. J. Thompson and R. E. Scholten, "Narrow linewidth tunable external cavity diode laser using wide bandwidth filter," Rev. Sci. Instrum. **83**, 023107 (2012).
18. S. G. Lynch, C. Holmes, S. A. Berry, J. C. Gates, A. Jantzen, T. I. Ferreiro, and P. G. R. Smith, "External cavity diode laser based upon an FBG in an integrated optical fiber platform," Opt. Express **24**, 8391–8398 (2016).
19. J. Lumeau, L. B. Glebov, and V. Smirnov, "Tunable narrow-band filter based on a combination of Fabry-Perot etalon and volume Bragg grating," Opt. Lett. **31**, 2417–2419 (2006).
20. O. Andrusyak, V. Smirnov, G. Venus, V. Rotar, and L. Glebov, "Spectral combining and coherent coupling of lasers by volume Bragg gratings," IEEE J. Sel. Top. Quantum **15**, 344–353 (2009).
21. X. Zhang, X. Yuan, S. Wu, J. Feng, K. Zou, and G. Zhang, "Two-dimensional angular filtering by volume Bragg gratings in photothermorefractive glass," Opt. Lett. **36**, 2167–2169 (2011).
22. Y. Wang, T. Kasamatsu, Y. Zheng, H. Miyajima, H. Fukuoka, S. Matsuoka, M. Niigaki, H. Kubomura, T. Hiruma, and H. Kan, "Cesium vapor laser pumped by a volume-Bragg-grating coupled quasi-continuous-wave laser-diode array," Appl. Phys. Lett. **88**, 141112 (2006).
23. D. Ott, I. Divliansky, B. Anderson, G. Venus, and L. Glebov, "Scaling the spectral beam combining channels in a multiplexed volume Bragg grating," Opt. Express **21**, 29620–29627 (2013).
24. G. Lucas-Leclin, P. Georges, J. Holm, M. T. Kelemen, B. Sumpf, and G. Erbert, "Wavelength stabilization of extended-cavity tapered lasers with volume Bragg gratings," Appl. Phys. B **91**, 493–498 (2008).
25. A. Gourevitch, G. Venus, V. Smirnov, and L. Glebov, "Efficient pumping of Rb vapor by high-power volume Bragg diode laser," Opt. Lett. **32**, 2611–2613 (2007).
26. B. L. Volodin, S. V. Dolgy, E. D. Melnik, E. Downs, J. Shaw, and V. S. Ban, "Wavelength stabilization and spectrum narrowing of high-power multimode laser diodes and arrays by use of volume Bragg gratings," Opt. Lett. **29**, 1891–1893 (2004).
27. D. Pabœuf, D. Vijayakumar, O. B. Jensen, B. Thestrup, J. Lim, S. Sujecki, E. Larkins, G. Lucas-Leclin, and P. Georges, "Volume Bragg grating external cavities for the passive phase locking of high-brightness diode laser arrays: theoretical and experimental study," J. Opt. Soc. Am. B **28**, 1289–1299 (2011).
28. R. Liu, B. Bo, N. Yao, Y. Xu, and X. Gao, "Experimental research on volume-Bragg-grating external-cavity red-light semiconductor lasers," Chin. J. Lumin. **40**, 1401–1408 (2019).
29. M. Niebuhr, C. Zink, A. Jechow, A. Heuer, L. B. Glebov, and R. Menzel, "Mode stabilization of a laterally structured broad area diode laser using an external volume Bragg grating," Opt. Express **23**, 12394–12400 (2015).
30. N. Ruhnke, A. Müller, B. Eppich, M. Maiwald, B. Sumpf, G. Erbert, and G. Tränkle, "Micro-integrated external cavity diode laser with 1.4-W narrowband emission at 445 nm," IEEE Photon. Technol. Lett. **28**, 2791–2794 (2016).
31. C. Moser, L. Ho, and F. Havermeyer, "Self-aligned non-dispersive external cavity tunable laser," Opt. Express **16**, 16691–16696 (2008).
32. C. Moser, L. Ho, and F. Havermeyer, "A novel tunable diode laser using volume holographic gratings," Proc. SPIE **7193**, 71930V (2009).
33. M. S. Akselrod, A. E. Akselrod, S. S. Orlov, S. Sanyal, and T. H. Underwood, "Fluorescent aluminum oxide crystals for volumetric optical data storage and imaging applications," J. Fluoresc. **13**, 503–511 (2003).
34. Y. Zhang, H. Dong, R. Wang, J. Duan, A. Shi, Q. Fang, and Y. Liu, "Demonstration of a home projector based on RGB semiconductor lasers," Appl. Opt. **51**, 3584–3589 (2012).
35. J. Cai, C. Lv, and A. Watanabe, "Cost-effective fabrication of high-performance flexible all-solid-state carbon micro-supercapacitors by blue-violet laser direct writing and further surface treatment," J. Mater. Chem. A **4**, 1671–1679 (2016).
36. P. Mueller, M. Thiel, and M. Wegener, "3D direct laser writing using a 405 nm diode laser," Opt. Lett. **39**, 6847–6850 (2014).
37. K. Ono, Y. Sato, R. Higashino, Y. Funada, N. Abe, and M. Tsukamoto, "Pure copper rod formation by multibeam laser metal deposition method with blue diode lasers," J. Laser Appl. **33**, 012013 (2021).
38. I. V. Ciapurin, L. B. Glebov, and V. I. Smirnov, "Modeling of Gaussian beam diffraction on volume Bragg gratings in PTR glass," Proc. SPIE **5742**, 183–194 (2005).
39. H. Kogelnik, "Coupled wave theory for thick hologram grating," Bell Syst. Tech. J. **48**, 2909–2945 (1969).
40. G. B. Venus, A. Sevian, V. I. Smirnov, and L. B. Glebov, "High-brightness narrow-line laser diode source with volume Bragg-grating feedback," Proc. SPIE **5711**, 166–176 (2005).